Electromagnon excitation in the field-induced noncollinear ferrimagnetic phase of $Ba_2Mg_2Fe_{12}O_{22}$ studied by polarized inelastic neutron scattering and terahertz time-domain optical spectroscopy

Taro Nakajima,[1,*] Youtarou Takahashi,[2,3] Shunsuke Kibayashi,[2] Masaaki Matsuda,[4] Kazuhisa Kakurai,[1,5] Shintaro Ishiwata,[2] Yasujiro Taguchi,[1] Yoshinori Tokura,[1,2] and Taka-hisa Arima[1,6]

[1]*RIKEN Center for Emergent Matter Science (CEMS), Saitama 351-0198, Japan.*
[2]*Department of Applied Physics and Quantum Phase Electronics Center (QPEC), University of Tokyo, Tokyo 113-8656, Japan*
[3]*PRESTO, Japan Science and Technology Agency, Chiyoda, Tokyo 102-8666, Japan.*
[4]*Quantum Condensed Matter Division, Oak Ridge National Laboratory, Oak Ridge, Tennessee 37831, USA*
[5]*Quantum Beam Science Center, Japan Atomic Energy Agency, Tokai, Ibaraki 319-1195, Japan*
[6]*Department of Advanced Materials Science, University of Tokyo, Kashiwa 277-8561, Japan*

We have studied magnetic excitations in a field-induced noncollinear commensurate ferrimagnetic phase of $Ba_2Mg_2Fe_{12}O_{22}$ by means of polarized inelastic neutron scattering (PINS) and terahertz (THz) time-domain optical spectroscopy under magnetic field. A previous THz spectroscopy study reported that the field-induced phase exhibits electric-dipole-active excitations with energies of around 5 meV [Kida *et al.*, Phys. Rev. B **83**, 064422 (2011)]. In the present PINS measurements, we observed inelastic scattering signals around 5 meV at the zone center in the spin-flip channel. This directly shows that the electric-dipole-active excitations are indeed of magnetic origin, that is, *electromagnons*. In addition, the present THz spectroscopy confirms that the excitations have oscillating electric polarization parallel to the c axis. In terms of the spin-current model (Katsura-Nagaosa-Balatsky model), the noncollinear magnetic order in the field-induced phase can induce static electric polarization perpendicular to the c axis, but not dynamic electric polarization along the c axis. We suggest that the electromagnon excitations can be explained by applying the magnetostriction model to the out-of-phase oscillations of the magnetic moments, which is deduced from the present experimental results.

PACS numbers: 75.30.Ds, 78.70.Nx, 75.80.+q, 75.85.+t

INTRODUCTION

Multiferroic hexaferrites have been extensively investigated because they exhibit spin-driven ferroelectricity associated with noncollinear magnetic orders in relatively low magnetic field and high temperature regions [1–7]. In fact, distinct magnetoelectric (ME) effects have been observed up to room temperature in a Z-type hexaferrite $Sr_3Co_2Fe_{24}O_{41}$ [5] and a Y-type hexaferrite $BaSrCo_{2-x}Zn_xFe_{11}AlO_{22}$ [7]. They are considered to be potential candidates for new electronic devices.

$Ba_2Mg_2Fe_{12}O_{22}$ (BMFO) to be investigated here is another multiferroic Y-type hexaferrite [2, 3, 8, 9]. Figure 1(a) shows the crystal structure of this system, which belongs to a rhombohedral space group of $R\bar{3}m$. Note that in this paper, we employ a conventional hexagonal basis for this structure. The lattice constants are $a = b = 5.88$ Å, and $c = 43.52$ Å. At room temperature, BMFO is in a paraelectric ferrimagnetic (FR) phase. With decreasing temperature in zero magnetic field, it first undergoes a magnetic transition from the ferrimagnetic phase to a screw-type helimagnetic phase with an incommensurate modulation parallel to the c axis at $T_N = 195$ K [10–12]. With further decreasing temperature, spontaneous magnetization appears along the c axis around $T_c \sim 50$ K in addition to the screw-type magnetic modulation. As a result, Fe spins are arranged in a longitudinal conical (LC) structure. By applying a magnetic field perpendicular to the c axis below T_c, the system displays several field-induced magnetic phases [8, 9]. In magnetic fields lower than ~ 0.06 T, the cone axis is canted from the c axis toward the direction of the applied magnetic field, and thus the LC structure is deformed into a transverse conical structure. In a relatively high field between 0.2 T and 4 T, a noncollinear commensurate ferrimagnetic phase with a magnetic modulation wave vector of $(0, 0, 3/2)$ emerges. In accordance with a previous neutron diffraction study by Ishiwata *et al.* [8], we refer to this phase as the FE3 phase. These field-induced intermediate magnetic phases host electric polarization perpendicular to both the magnetic field and the modulation wave vector. With further increasing magnetic field, the system ends up with the field-induced FR phase. The spin-driven electric polarization vanishes at the phase transition from the FE3 phase to the FR phase.

To pin down the microscopic origin of the spin-driven ferroelectricity, it is necessary to determine the magnetic structures in these phases. However, a large number of magnetic Fe^{3+} ions in a unit cell and partial mixing of Fe^{3+} and Mg^{2+} sites make it unpractical to determine the directions of all the magnetic moments in the magnetically ordered phases. Instead, in previous studies, the magnetic structures are approximately represented by using two kinds of ferrimagnetically-ordered blocks, which are alternately stacked along the c axis [11, 12].

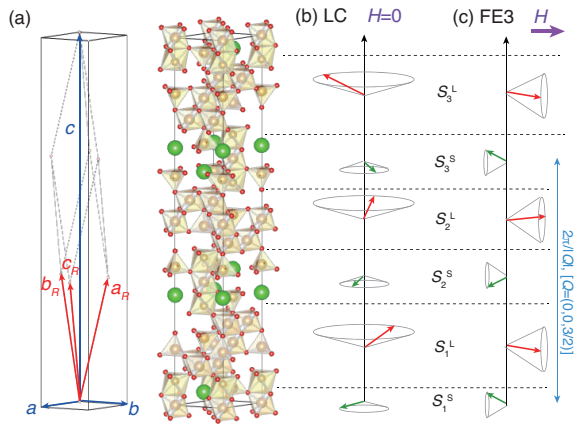

FIG. 1: (Color online) (a) The crystal structure of $Ba_2Mg_2Fe_{12}O_{22}$, the hexagonal basis (a, b, c) and rhombohedral basis (a_R, b_R, c_R). Schematic models of magnetic structures in the (b) LC and (c) FE3 phases, depicted on the basis of the block approximation.

The blocks are referred to as 'L block' and 'S block', which have larger and smaller net magnetic moments, respectively [2, 8]. In this paper, we treat these magnetic moments as classical spins, and refer to the net magnetic moment of ith L (S) block as S_i^L (S_i^S). On the basis of this block approximation, we can schematically depict the magnetic structures in zero and applied magnetic fields, as shown in Figs. 1(b) and 1(c), respectively. The emergence of electric polarization can be qualitatively explained by applying the formula proposed by Katsura, Nagaosa and Baratsky (KNB), $P \propto e_{i,j} \times (S_i \times S_j)$, where $e_{i,j}$ is a unit vector connecting between two neighboring spins, S_i and S_j [13–15], to the schematic models of the magnetic structures.

In addition to the static ME coupling mentioned above, BMFO is also known to exhibit dynamical ME coupling, namely gigantic magnetochromism in terahertz frequency region. Kida *et al.* observed strong optical absorption associated with the magnetic orders, in an energy range of 3 ∼ 5 meV [16, 17]. They performed optical spectroscopy measurements with various configurations of the incident light polarization with respect to the crystallographic axes, concluding that the origin of the absorption is electric-dipole-active magnetic resonance, namely 'electromagnon' excitation.

The electromagnon excitations have been reported in a variety of spin-driven multiferroics such as orthorhombic $R\mathrm{MnO_3}$ [18–21], $R\mathrm{Mn_2O_5}$ [22, 23] (R is a rare-earth element), CuO [24, 25] etc., and have attracted much attention because of the possibility for new optoelectronic applications. The most naive interpretation of the electromagnon excitations might be that an electric-field component of the incident light (E^ω) is coupled with the magnons via the same mechanism as that for the spin-driven static electric polarizations. However, subsequent spectroscopic and theoretical studies on the multiferroics [21, 26–30] have revealed that the static and dynamical ME couplings in a spin-driven multiferroic material can have different origins. In fact, in BMFO, the large absorption was also observed in the zero-field LC phase, which is not accompanied by ferroelectricity [16, 17]. Moreover, previous THz spectroscopy studies revealed that the electromagnon excitation in BMFO is observed only when E^ω is parallel to the c axis [16, 17], while the KNB formula does not allow the electric polarization to have a component along the magnetic modulation wave vector. This indicates that the origin of the large optical absorption cannot be explained by the KNB formula. Instead, Kida *et al.* proposed the exchange-striction mechanism, in which the optical activity is explained in terms of structural modulations induced by the temporal change of the Heisenberg exchange coupling $S_i \cdot S_j$ [16]. Note that the exchange-striction mechanism also successfully explained the electromagnon excitations in $R\mathrm{MnO_3}$ [19–21] and $R\mathrm{Mn_2O_5}$ [23, 26].

To investigate the dynamical coupling between spin moments and electric polarization in BMFO in more detail, we directly observe the spin dynamics by means of polarized inelastic neutron scattering. By using this technique, we can extract magnetic excitations which have spin components oscillating perpendicular to the polarization direction of incident neutrons from inelastic spin-flip scattering spectra [31]. However, this technique is not applicable to the zero-field LC phase. This is because the spins of the incident neutrons are easily depolarized when the system has non-uniform ferromagnetic components. In the present study, we focus on the FE3 phase, in which the direction of the uniform magnetization is fixed to be parallel to the applied magnetic field. Another reason to focus on the FE3 phase is that the optical absorption is significantly enhanced in this phase [16]. We performed polarized inelastic neutron scattering measurements in a magnetic field of 1 T applied perpendicular to the c axis.

We also performed THz time-domain spectroscopy on BMFO under magnetic fields applied perpendicular to the c axis. Although THz absorption spectra have already been measured under magnetic fields in the configuration of $E^\omega \| [001]$ [16], we investigated the light-polarization dependence under magnetic fields, which can be directly compared with the inelastic neutron scattering data. Combining results of the THz optical spectroscopy and polarized inelastic neutron scattering measurements, we discuss the microscopic mechanism of the dynamical ME effect in this system.

EXPERIMENTS

Single crystals of BMFO were grown by flux growth technique [12]. Three large crystals of BMFO (total mass

of 1.81 g) were carefully co-aligned in a sample holder by using the high-energy x-ray transmission Laue camera installed in Institute of Solid State Physics, the University of Tokyo, Japan. Polarized inelastic neutron scattering measurements were carried out at the triple-axis neutron spectrometer PTAX installed at the horizontal beamtube HB-1 in the High Flux Isotope Reactor of Oak Ridge National Laboratory. The samples were loaded into a vertical-field cryomagnet with a maximum field of 7 T. We applied a *dc* magnetic field (H^{dc}) parallel to the [100] direction. An incident polarized neutron beam was obtained by a Heusler (111) monochromator. The collimation was 48′-80′-80′-open. The direction of the neutron spin polarization was set to be parallel or antiparallel to the applied magnetic field, by a spin flipper placed between the monochromator and the cryomagnet. We employed a pyrolytic graphite (002) and a Heusler (111) analyzers to efficiently survey dispersion relations of the magnetic excitations without polarization analysis, and to perform the polarization analysis for the scattered neutrons, respectively. The flipping ratio of the polarized neutron beam was ~ 13. The spectrometer operated in the fixed-E_f mode with E_f (the energy of scattered neutrons) of 13.5 meV. The energy resolution at the elastic condition was 1.2 meV.

We also performed time-domain THz spectroscopy under magnetic field. The laser pulses from Ti:sapphire laser with 80 MHz repetition rate was split into two paths to generate and detect the THz pulses. A bow-tie shaped antenna was used to generate the THz pulse, while the dipole antenna was used for detection. The energy resolution was about 0.4 meV. We applied magnetic field in two configurations by a superconducting magnet. In the Faraday geometry, where the propagation vector of light k is parallel to H^{dc}, the optical response for $E^{\omega}\|[001]$, $H^{dc}\|[100]$ [see Fig. 2(a)] was measured. On the other hand, the optical response for $E^{\omega}\|[100]$, $H^{dc}\|[100]$ [see Fig. 2(b)] was measured in the Voigt geometry, where k is perpendicular to H^{dc}.

RESULTS AND DISCUSSIONS

THz time-domain spectroscopy

Figures 2(c)-2(e) show spectra of ϵ_2 (imaginary part of dielectric constant) under the magnetic field along [100] below 7 T. The electrically active excitations with clear peak structures show up around $3 \sim 5$ meV, whose polarization is always $E^{\omega}\|[001]$, while the spectral shape exhibits noticeable magnetic field dependence. On the other hand, no discernible excitation for $E^{\omega}\|[100]$ was observed in the current energy window. Note that in the present study, we carefully evaluated the signal-to-noise ratio of raw data and the accuracy of complex dielectric spectra obtained from them. Due to the low transmittance around the main peak in the FE3 phase, we have omitted the data around 5 meV in the FE3 phase [see Fig. 2(d)]. Except for this point, the polarization character as well as the magnetic field variations of the THz spectra are consistent with those in the early works by Kida *et al.*, [16, 17].

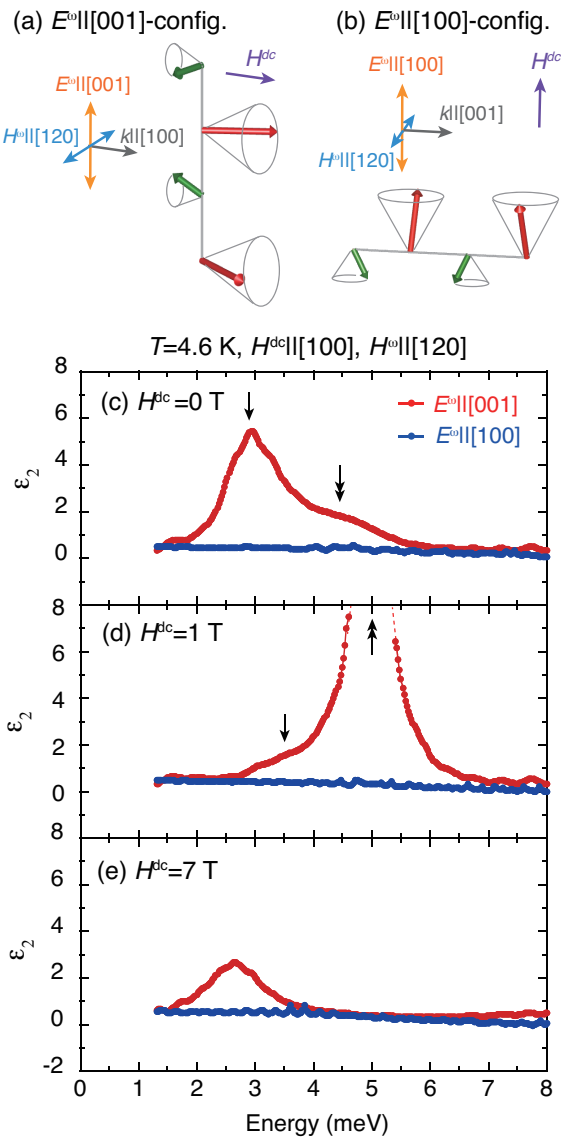

FIG. 2: (Color online) Schematics showing the relationships among the directions of the incident light wave, electric-field and magnetic-field components of the light, magnetic moments, and the dc magnetic field for the (a) $E^{\omega}\|[001]$- and (b) $E^{\omega}\|[100]$-configurations. Spectra of the imaginary part of the dielectric constant obtained from the time-domain THz spectroscopy under the magnetic field along [100] with (c) 0, (d) 1 and (e) 7 T at 4.6 K. Red and blue lines show the spectra measured in the $E^{\omega}\|[001]$- and $E^{\omega}\|[100]$-configurations, respectively. The single and double black arrows show the positions of the peaks (see the main text for details).

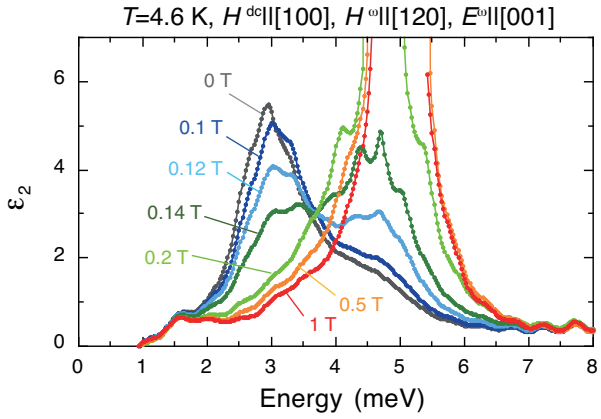

FIG. 3: (Color online) Magnetic field dependence of the imaginary part of the dielectric constant between 0 and 1 T measured by the THz optical spectroscopy with the $E^{\omega}\|[001]$ configuration.

In the LC phase at zero field in Fig. 2(c), we observed a peak around 3 meV and a shoulder around 4.5 meV in the $E^{\omega}\|[001]$-configuration as indicated by single and double arrows, respectively. The electromagnon resonance develops with increasing magnetic field as observed in the spectra at 1 T. Further increase of the magnetic field suppresses the electromagnon resonance, while the resonance still remained in the field-induced FR phase at 7 T [see Fig. 2(e)].

By measuring magnetic field dependence of the spectra between 0 and 1 T in detail, we have found that the main peak in the LC phase (at 0 T) are suppressed with increasing magnetic field, and finally, turned into a shoulder peak around 3.5 meV in the FE3 phase, as shown in Fig. 3. On the other hand, the shoulder in the LC phase turned into the main peak at 5 meV in the FE3 phase.

Inelastic neutron scattering measurements in FE3 phase

We surveyed dispersion relations of magnetic excitations along the c^* axis in the unpolarized condition. Figure 4 shows constant-Q scans measured at a number of reciprocal lattice points along the $(0, 0, L)$ line at 1.5 K under applied magnetic field of 1 T. We observed a broad peak around 5 meV for all the inelastic scattering spectra, some of which also have shoulders. This energy roughly agrees with the peak energy of the THz optical spectrum. Although these peaks are slightly shifted toward higher energies as compared to those in the optical spectra, this should be attributed to the resolution effect of the triple-axis neutron spectrometer.

We found that the peak positions in the inelastic scattering spectra do not show remarkable L dependence.

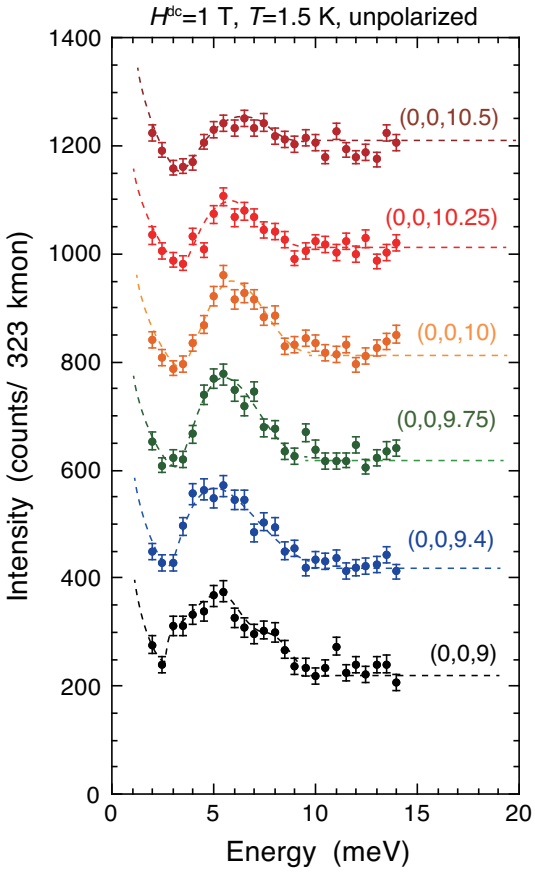

FIG. 4: (Color online) Unpolarized inelastic neutron scattering spectra measured by constant-Q scans at reciprocal lattice points along the $(0, 0, L)$ line, at $H^{dc} = 1$ T and $T = 1.5$ K. The monitor counts of 323,000 corresponds to 320 $\sim$ 400 seconds in the energy range of 0 $\sim$ 14 meV. Note that the data are shifted by 200 for each, to enhance the visibility. The dashed lines are guides to the eyes.

This is in contrast to the steep spin-wave dispersion perpendicular to the c axis observed in the previous inelastic neutron scattering study in the zero-field LC phase [17]. The present results suggest that the exchange interaction along the c axis, specifically the interaction connecting the adjacent ferrimagnetic blocks, are relatively weak as compared to the interactions perpendicular to the c axis.

Next, we performed polarized neutron scattering measurements in the FE3 phase. Here, we introduce Cartesian coordinates xyz to describe the relationship among the directions of the neutron spin polarization ($\boldsymbol{p}_N$), magnetic moments in the sample and the crystallographic axes of the sample, as shown in Fig. 5(d); the x, y and z directions are defined to be parallel to the [120], [001] and [100] directions, respectively. In neutron scattering experiments, the magnetic scattering cross section is proportional to a square of Fourier-transformed magnetic moments projected on a plane perpendicular to the

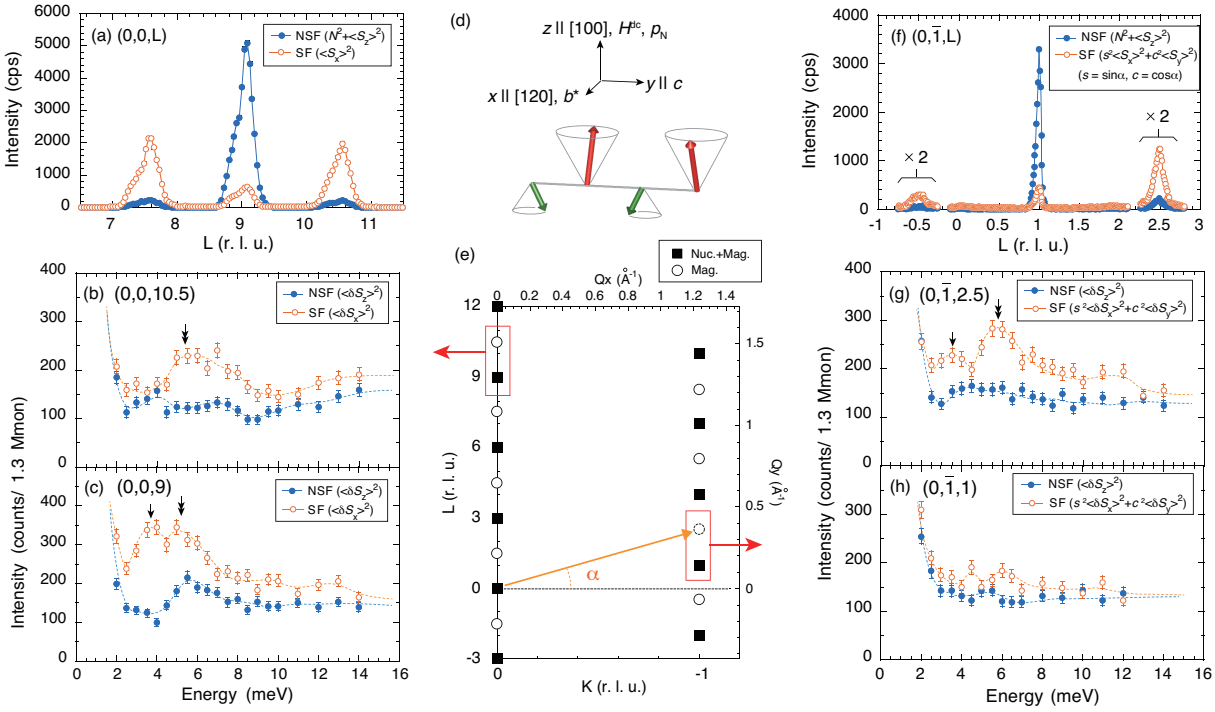

FIG. 5: (Color online) (a) The polarized neutron diffraction profile along the $(0, 0, L)$ line at $H^{dc} = 1$ T and $T = 1.5$ K. [(b),(c)] The polarized inelastic scattering spectra at (b) (0,0,10.5) and (c) (0,0,9). (d) A schematic showing the relationship among the cartesian coordinate xyz, the directions of the magnetic moments, dc magnetic field, neutron polarization, and crystallographic axes. (e) The reciprocal lattice map of the $(0, K, L)$ scattering plane. (f) The polarized neutron diffraction profile along the $(0, \bar{1}, L)$ line. [(g),(h)] The polarized inelastic scattering spectra at (b) (0,$\bar{1}$,2.5) and (c) (0,$\bar{1}$,1). In Figs. (a)-(c) and (f)-(h), open and filled symbols show the intensities measured in the SF and NSF channel, respectively. The monitor counts of 1.3 million corresponds to 1200 $\sim$ 1600 seconds in the energy range of 0 $\sim$ 14 meV. The dashed lines are guides to the eyes. The vertical single and doubled arrows show the peak positions corresponding to the two peaks around 3 and 5 meV observed in the THz absorption spectra, respectively.

scattering vector, $\boldsymbol{\kappa}(= \boldsymbol{k}_i - \boldsymbol{k}_f)$. For example, when the scattering vector is parallel to the y direction, namely the c^* axis, we observe the x and z components of the Fourier-transformed magnetic moments. By using polarized neutrons, we can distinguish these components; specifically, when $\boldsymbol{p}_N$ is parallel to the z direction, the x and z components are observed in spin-flip (SF) and non-spin-flip (NSF) channels, respectively [31].

Figures 5(a) and 5(f) show diffraction profiles along the $(0, 0, L)$ and $(0, \bar{1}, L)$ lines, respectively. Open and filled symbols show intensities observed in the SF and NSF channels, respectively. We observed strong peaks at (0,0,9) and (0,$\bar{1}$,1) in the NSF channel. In addition, satellite reflections at (0,0,9)$\pm(0, 0, 3/2)$ and (0,$\bar{1}$,1)$\pm(0, 0, 3/2)$ were observed in the SF channel. This is because the magnetic structure in the FE3 phase consists of a collinear ferrimagnetic component with $\boldsymbol{Q} = (0, 0, 0)$ along the z direction and a cycloidal modulation with $\boldsymbol{Q} = (0, 0, 3/2)$ in the xy plane, as was reported by Ishiwata *et al.* [8]. Note that the 009 and 0$\bar{1}$1 reflections also contain nuclear scattering signals, which are observed only in the NSF channel.

At the reciprocal lattice points of (0,0,9) and (0,0,10.5), both of which correspond to the zone center for the magnetic unit cell in the FE3 phase, we performed constant-Q scans with polarization analysis. Similarly to the elastic scattering mentioned above, the inelastic SF signals at $(0, 0, L)$ are attributed to the spin components oscillating along the x direction, while the inelastic NSF signals account for the spin components oscillating along the z direction and/or phonon excitations. As shown in Figs. 5(b) and 5(c), we found that the inelastic scattering signals at 3 $\sim$ 5 meV mainly come from the SF channel. This demonstrates that these excitations are indeed of magnetic origin, because the SF scatterings occur only from magnetic excitations. The sums of the SF and NSF signals are consistent with the unpolarized spectra, taking into account difference in reflectivity between the PG and Heusler analyzers.

We also performed constant-Q scans at (0,$\bar{1}$,2.5) and (0,$\bar{1}$,1), as shown in Figs. 5(g) and 5(h). At (0,$\bar{1}$,2.5), two peaks were observed at about 3 and 5 meV in the SF channel, similarly to the constant-Q spectra along the $(0, 0, L)$ line. Because $\boldsymbol{\kappa}$ was not parallel to the x or y

direction at (0,$\bar{1}$,2.5), both of the x and y components can contribute to the scattering cross section. If the x and y components have the same oscillating amplitude as each other, their contributions to the inelastic scattering signals are roughly estimated to be proportional to $\delta S^2 \sin^2\alpha$ and $\delta S^2 \cos^2\alpha$, respectively, where δS is the oscillating amplitude and α is an angle between $\boldsymbol{\kappa}$ and the b^* axis (x direction). Taking into account that $\tan^2\alpha = 0.086$ ($\alpha = 16.3°$) at (0,$\bar{1}$,2.5), we consider that the SF scattering at (0,$\bar{1}$,2.5) is mainly attributed to the magnetic moments oscillating along the y direction.

These results confirmed that the excitations at 3 $\sim$ 5 meV are indeed magnetic excitations, which correspond to oscillations of the magnetic moments mainly in the xy plane.

Microscopic model for the dynamical magneto-electric coupling

To reveal the microscopic origin of the electromagnon excitations, it is necessary to establish microscopic pictures of the spin-wave modes. However, because of the existence of a large number of Fe^{3+} ions and the site mixing with the Mg^{2+} ions, it is quite difficult to exactly determine the oscillating directions and amplitudes of each magnetic moment in the unit cell. Instead, in the following, we focus only on the zone-center excitations, which are relevant to the optical responses, and qualitatively interpret the oscillating directions and their phase relationships, on the basis of the present results.

Here, we introduce two simplified modes at the zone center referred to as 'in-phase oscillation' and 'out-of-phase oscillation', respectively; in the former, the temporal deviations of S_1^L and S_2^L (S_1^S and S_2^S) are in phase, while in the later, they are out of phase. In Figs. 6(a) and 6(b), we schematically illustrate the y components of the deviations of the magnetic moments in the two types of oscillations. Note that in the in-phase oscillation, the deviations of S_1^L and S_1^S are assumed to be opposite to each other. If S_1^L and S_1^S would oscillate in phase, then this mode would have net oscillating magnetization, which would be observed by the THz optical spectroscopy regardless of the polarization of E^ω.

The in-phase oscillation has the same periodicity as that of the crystal lattice, and therefore the inelastic scattering signals from this mode should be mainly observed at nuclear Bragg points. On the other hand, in the out-of-phase mode, the deviations of the magnetic moments are characterized by the wave vector of $\boldsymbol{Q} = (0, 0, 3/2)$. Therefore, this mode mainly contributes to the inelastic scattering signals measured at magnetic Bragg points.

For example, the inelastic SF scattering spectrum at (0,0,9) indicates that the x components of the magnetic moments show the in-phase oscillations at energies of about 3 and 5 meV. We also observed the SF scattering

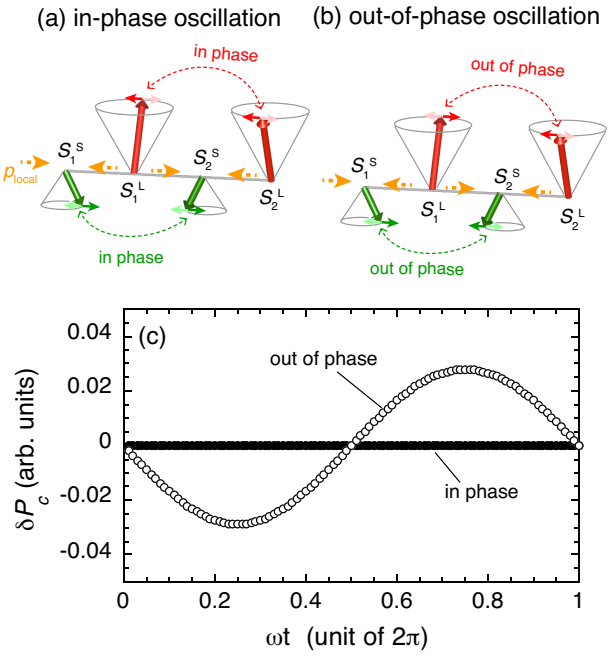

FIG. 6: (Color online) Schematic pictures of (a) 'in-phase' and (b) 'out-of-phase' oscillations of the y (c-axis) component of the magnetic moments. Horizontal orange dotted arrows denote the local electric dipole moments ($p_{\rm local}$) embedded in the crystal structure. (c) Calculated values of δP_c for the in-phase and out-of-phase oscillations.

with the energy of $\sim$ 5 meV at (0,0,10.5), which indicates that there also exists the out-of-phase oscillation of the x components with the energy. Similarly, the inelastic SF scattering spectrum at (0,$\bar{1}$,2.5) shows that the y components of the magnetic moments exhibits the out-of-phase oscillations with the energies of about 3 and 5 meV. It should be noted that we also observed small inelastic scattering signals in the NSF channel around 5 meV at (0,0,9), suggesting the existence of in-phase oscillation of the z components of the magnetic moments or phonon excitation.

As was mentioned in the introduction, the KNB formula can explain neither static nor dynamic electric polarization component along the c axis. Therefore, we employ the magnetostriction, which was also used to explain the electromagnon excitations in the LC phase in the previous work [16]. Here, we define local electric dipole moments ($p_{\rm local}$) between the L and S blocks, which originates from the crystal structure, specifically the lacking of inversion symmetry between the L and S blocks, as shown in Figs. 6(a) and 6(b). Because the system does not have spontaneous electric polarization along the c axis, neighboring electric dipole moments should have the same magnitude but opposite signs. We assume that these dipole moments are modified by the magnetic ordering; specifically, the changes in magnitude of p_{local} are

assumed to be proportional to exchange coupling $S \cdot S$ between neighboring L and S blocks. Therefore, the net electric polarization along the c axis is described as:

$$P_c \propto \boldsymbol{S}_1^S \cdot \boldsymbol{S}_1^L - \boldsymbol{S}_1^L \cdot \boldsymbol{S}_2^S + \boldsymbol{S}_2^S \cdot \boldsymbol{S}_2^L - \boldsymbol{S}_2^L \cdot \boldsymbol{S}_1^S \quad (1)$$

In the static limit, all $S^L \cdot S^S$ values are the same as each other, and therefore the macroscopic electric polarization along the c axis is not induced by magnetostriction. By substituting temporal deviations of the magnetic moments into Eq. (1), we can explain the emergence of the oscillating electric polarization along the c axis, as follows. For simplicity, we focus on the y components of the magnetic moments. To calculate $P_c(t)$ for the in-phase and out-of-phase oscillations of the y component, we assumed that the oscillation of each magnetic moment as follows:

$$\boldsymbol{S}_i^{S/L}(t) = \langle \boldsymbol{S}_i^{S/L} \rangle + \delta S^{S/L} \sin(\omega t - \phi_i^{S/L}) \mathbf{e}_y, \quad (2)$$

where $\langle \boldsymbol{S}_i^{S/L} \rangle$ shows the mean direction and length of the net magnetic moment at ith S/L block. $\mathbf{e}_y$ is a unit vector along the y direction. The amplitude of the oscillation at the ith S/L block, $\delta S^{S/L}$, is assumed to be one order of magnitude smaller than the length of $\langle \boldsymbol{S}_i^{S/L} \rangle$. For the in-phase oscillation, the phases of the four spins should be $\phi_1^L = \phi_2^L = 0$ and $\phi_1^S = \phi_2^S = \pi$. Similarly, we defined the phases for the out-of-oscillation as follows: $\phi_1^L = \phi_1^S = 0$ and $\phi_2^S = \phi_2^L = \pi$. By substituting Eq. (2) into Eq. (1), we calculated δP_c for the two oscillations, as shown in Fig. 6(c), revealing that the out-of-phase oscillation of the magnetic moments induces an oscillation of P_c whose period is the same as that of the oscillation of the magnetic moments. The oscillating δP_c can be coupled with E^ω of the incident light wave, resulting in the electromagnon excitations. By contrast, the in-phase oscillation does not induce δP_c. Note that in this calculation, we fixed $\delta S^S / \delta S^L$ at 1. However, we also confirmed that the presence and absence of the oscillating δP_c in the out-of-phase and in-phase oscillations still hold, respectively, regardless of the ratio between δS^S and δS^L.

In reality, the magnetic excitations consist of several components of the oscillating magnetic moments. In addition, because the magnetic unit cell for the FE3 phase contains a lot of Fe^{3+} ions, there should exist many spin-wave branches, some of which are overlapped with each other. Actually, the present PINS measurements revealed that the 'in-phase' and 'out-of-phase' oscillations coexist with each other around 3 to 5 meV. However, we emphasize that the out-of-phase modes are essential for the electromagnon excitations, but the in-phase modes are not. This is because the out-of-phase oscillation rotate S_1^L and S_2^L in opposite direction. This always induces a difference between $S_1^L \cdot S_1^S$ and $S_1^S \cdot S_2^L$, regardless of the direction of the deviation and the phase relationship between S_1^L and S_1^S. Therefore, we suggest that the 'out-of-phase' oscillations of the magnetic moments, which were in fact observed as the inelastic SF scattering signals at about 3 and 5 meV at $(0,\bar{1},2.5)$ and those at about 5 meV at (0,0,10.5), are relevant to the electromagnon excitations in the FE3 phase.

It should be noted here that Eq. (1) cannot explain the difference in optical absorption strength between the excitations at 3 and 5 meV. The present PINS results show that the magnetic moments are oscillating mainly along the y direction in the out-of-phase mode at 3 meV, while they are oscillating along the x and y directions in the excitation at 5 meV. Although these modes can induce different amplitudes of δP_c, we could not reproduce the observed THz spectra, in which the absorption at 5 meV is significantly larger than that at 3 meV, using Eq. (1). To fully explain the dynamical spin-polarization coupling in this system, we may need to improve our model and to apply it to more detailed pictures of the magnetic structures beyond the block approximation.

SUMMARY

In summary, we performed polarized inelastic neutron scattering measurements and THz time-domain optical spectroscopy on $Ba_2Mg_2Fe_{12}O_{22}$ under applied magnetic field, in order to investigate the origin of the electromagnon excitations in the noncollinear commensurate ferrimagnetic phase, namely the FE3 phase. In the THz spectroscopy experiments, we confirmed that the electromagnon excitations in the FE3 phase also have the oscillating electric polarization parallel to the c axis. We observed inelastic neutron scattering signals at about 3 to 5 meV at the zone center in the field-induced phase. By the polarization analysis, we revealed that the inelastic scattering signals mainly come from the spin-flip channel. This indicates that the excitations are indeed of magnetic origin, and that the magnetic moments are oscillating mainly perpendicular to the magnetic field. Applying the magnetostriction model to the schematic pictures of the oscillations of the magnetic moments deduced from the polarization analysis, we proposed that the 'out-of-phase' oscillation of the magnetic moments can induce oscillating electric polarization along the c axis, which is consistent with the electromagnon activity in the FE3 phase.

Acknowledgements

The neutron scattering experiment at ORNL's HFIR was conducted along the proposal No. IPTS-11376.1, and was sponsored by the Scientific User Facilities Division, Office of Basic Energy Sciences, US Department of En-

ergy. This study was supported in part by the U.S.-Japan Cooperative Program on Neutron Scattering. The images of the crystal and magnetic structures in this paper were depicted using the software VESTA [32] developed by K. Momma.

* Electronic address: taro.nakajima@riken.jp

[1] T. Kimura, G. Lawes, and A. P. Ramirez, Phys. Rev. Lett. **94**, 137201 (2005).
[2] S. Ishiwata, Y. Taguchi, H. Murakawa, Y. Onose, and Y. Tokura, Science **319**, 1643 (2008).
[3] K. Taniguchi, N. Abe, S. Ohtani, H. Umetsu, and T.-h. Arima, Appl. Phys. Express **1**, 031301 (2008).
[4] Y. S. Chai, S. H. Chun, S. Y. Haam, Y. S. Oh, I. Kim, and K. H. Kim, New Journal of Physics **11**, 073030 (2009).
[5] Y. Kitagawa, Y. Hiraoka, T. Honda, T. Ishikura, H. Nakamura, and T. Kimura, Nat. Mater. **9**, 797 (2010).
[6] S. H. Chun, Y. S. Chai, Y. S. Oh, D. Jaiswal-Nagar, S. Y. Haam, I. Kim, B. Lee, D. H. Nam, K.-T. Ko, J.-H. Park, et al., Phys. Rev. Lett. **104**, 037204 (2010).
[7] S. Hirose, K. Haruki, A. Ando, and T. Kimura, Appl. Phys. Lett. **104**, 022907 (2014).
[8] S. Ishiwata, D. Okuyama, K. Kakurai, M. Nishi, Y. Taguchi, and Y. Tokura, Phys. Rev. B **81**, 174418 (2010).
[9] H. Sagayama, K. Taniguchi, N. Abe, T.-h. Arima, Y. Nishikawa, S.-i. Yano, Y. Kousaka, J. Akimitsu, M. Matsuura, and K. Hirota, Phys. Rev. B **80**, 180419 (2009).
[10] J. Smit and H. P. J. Wijn, *Ferrites* (Philips Technical Library, Eindhoven, 1959).
[11] N. Momozawa, Y. Yamaguchi, and M. Mita, Journal of the Physical Society of Japan **55**, 1350 (1986).
[12] N. Momozawa, Y. Nagao, S. Utsumi, M. Abe, and Y. Yamaguchi, Journal of the Physical Society of Japan **70**, 2724 (2001).
[13] I. A. Sergienko and E. Dagotto, Phys. Rev. B **73**, 094434 (2006).
[14] H. Katsura, N. Nagaosa, and A. V. Balatsky, Phys. Rev. Lett. **95**, 057205 (2005).
[15] M. Mostovoy, Phys. Rev. Lett. **96**, 067601 (2006).
[16] N. Kida, S. Kumakura, S. Ishiwata, Y. Taguchi, and Y. Tokura, Phys. Rev. B **83**, 064422 (2011).
[17] N. Kida, D. Okuyama, S. Ishiwata, Y. Taguchi, R. Shimano, K. Iwasa, T. Arima, and Y. Tokura, Phys. Rev. B **80**, 220406 (2009).
[18] A. Pimenov, A. A. Mukhin, V. Y. Ivanov, V. D. Travkin, A. M. Balbashov, and A. Loidl, Nat. Phys. **2**, 97 (2006).
[19] R. Valdés Aguilar, M. Mostovoy, A. B. Sushkov, C. L. Zhang, Y. J. Choi, S.-W. Cheong, and H. D. Drew, Phys. Rev. Lett. **102**, 047203 (2009).
[20] J. S. Lee, N. Kida, S. Miyahara, Y. Takahashi, Y. Yamasaki, R. Shimano, N. Furukawa, and Y. Tokura, Phys. Rev. B **79**, 180403 (2009).
[21] N. Kida, Y. Takahashi, J. S. Lee, R. Shimano, Y. Yamasaki, Y. Kaneko, S. Miyahara, N. Furukawa, T. Arima, and Y. Tokura, J. Opt. Soc. Am. B **26**, A35 (2009).
[22] A. B. Sushkov, R. V. Aguilar, S. Park, S.-W. Cheong, and H. D. Drew, Phys. Rev. Lett. **98**, 027202 (2007).
[23] J.-H. Kim, M. A. van der Vegte, A. Scaramucci, S. Artyukhin, J.-H. Chung, S. Park, S.-W. Cheong, M. Mostovoy, and S.-H. Lee, Phys. Rev. Lett. **107**, 097401 (2011).
[24] S. P. P. Jones, S. M. Gaw, K. I. Doig, D. Prabhakaran, E. M. Hétroy Wheeler, A. T. Boothroyd, and J. Lloyd-Hughes, Nat. Commun. **5** (2014).
[25] K. Cao, F. Giustino, and P. G. Radaelli, Phys. Rev. Lett. **114**, 197201 (2015).
[26] A. B. Sushkov, M. Mostovoy, R. V. Aguilar, S.-W. Cheong, and H. D. Drew, J. Phys.:Condens. Matter **20**, 434210 (2008).
[27] M. Mochizuki, N. Furukawa, and N. Nagaosa, Phys. Rev. Lett. **104**, 177206 (2010).
[28] R. Valdés Aguilar, A. B. Sushkov, C. L. Zhang, Y. J. Choi, S.-W. Cheong, and H. D. Drew, Phys. Rev. B **76**, 060404 (2007).
[29] A. Pimenov, A. Shuvaev, A. Loidl, F. Schrettle, A. A. Mukhin, V. D. Travkin, V. Y. Ivanov, and A. M. Balbashov, Phys. Rev. Lett. **102**, 107203 (2009).
[30] N. Kida, Y. Ikebe, Y. Takahashi, J. P. He, Y. Kaneko, Y. Yamasaki, R. Shimano, T. Arima, N. Nagaosa, and Y. Tokura, Phys. Rev. B **78**, 104414 (2008).
[31] R. M. Moon, T. Riste, and W. C. Koehler, Phys. Rev. **181**, 920 (1969).
[32] K. Momma and F. Izumi, J. Appl. Crystallogr. **41**, 653 (2008).